Applied Catalysis B: Environmental 127 (2012) 121–128

Contents lists available at SciVerse ScienceDirect

Applied Catalysis B: Environmental

journal homepage: www.elsevier.com/locate/apcatb

HAN and ADN as liquid ionic monopropellants: Thermal and catalytic decomposition processes

Rachid Amrousse[a,*], Keiichi Hori[a], Wafa Fetimi[b], Kamal Farhat[c]

[a] Japan Aerospace Exploration Agency (JAXA), 3-1-1 Yoshinodai, Chuo-Ku, Sagamihara, Kanagawa 252-5210, Japan
[b] M2P2, Laboratoire de Mécanique, Modélisation & Procédés Propres, UMR-CNRS 6181, Université Aix Marseille, 13451 Marseille Cedex 13, France
[c] IC2MP, Institut de Chimie des Milieux et des Matériaux, University of Poitiers, 86022 Poitiers, France

ARTICLE INFO

Article history:
Received 4 May 2012
Received in revised form 30 June 2012
Accepted 13 August 2012
Available online 20 August 2012

Keywords:
Monopropellant
HAN
ADN
Catalytic decomposition process

ABSTRACT

Binary HAN and ADN aqueous solutions have been synthesized, then thermally and catalytically decomposed. Binary HAN mixtures were prepared with different concentrations: 95, 80 and 60 wt.%. Whereas ADN solution contains are: 75, 60 and 50 wt.%. The candidate catalysts were prepared by impregnation of alumina doped by lanthanum oxide with active phase precursors: iridium for HAN and copper oxide for ADN and characterized by transmission electron microscopy, X-ray diffraction and chemisorption. The decomposition processes were followed by thermal analysis and a constant batch reactor. This work shows the essential effect of monopropellant concentrations to determine the best green propellants for industrial applications as reaction control systems. Moreover, HAN and ADN solutions are more efficient for catalytic decomposition due to the absence of stabilizer to inhibit catalysts. The (10%)Ir/Al_2O_3–La_2O_3 + $HAN_{95\%}$ and the (10%)CuO/Al_2O_3–La_2O_3 + $ADN_{75\%}$ associations show lower decomposition temperatures, larger reaction rates and leads to higher amount of gas phase products, giving the most efficient systems.

1. Introduction

Energetic liquid compounds known as monopropellants are used for propulsion and gas generator purposes [1]. The conventional monopropellant is hydrazine, but the high vapor pressure of hydrazine and its high toxicity cause high storage and handling costs. Thus, the replacement of hydrazine by a less toxic propellant is desired. Hydroxyl ammonium nitrate (HAN) is a promising substitute for hydrazine because of its low toxicity, high density, high specific impulse, and low freezing point [2]. The key point in the use of HAN as a monopropellant is to find a highly active catalyst that can decompose HAN at low temperature. Recently, progress has been made in this area although ignition at ambient temperature has not yet been realized [1,3–5]. Aqueous ionic propellants are difficult to decompose and the development of a catalyst support capable of withstanding temperature near 1300 °C without significant loss of surface area remains a challenge. The concept of AMCAT (Advanced Monolithic CATalyst) has been proposed [6], but no information about catalytic bed and propellant formulation has been given. Eleven proprietary catalysts showed reactivity at temperature less than 60 °C and two catalysts at room temperature, but no information was given on the evaluation tests or on the propellant used for these tests. Catalyst support with stabilizing agent sustains 2 h at 1280 °C with a final surface area of 44 $m^2\,g^{-1}$. The conclusions are: (i) development of catalysts for a particular propellant formulation and it is not safe to assume that a catalyst which works well with one propellant will work well with another one; (ii) development of new materials that can tolerate longer exposure to high temperature without significant sintering. A more recent paper [7] focuses on propellants using methanol (HAN269MEO) or tris(2-aminoethyl)amine trinitrate $N{-}(C_2H_4NH_3)_3{}^{3+}{\cdot}3NO_3{}^-$ (HAN269TRN) as fuels. Nevertheless, reliable catalytic ignition still requires a preheating temperature of 400 °C to achieve stable and smooth combustion and the challenge is to reduce this temperature down to 100 °C. On the other hand, in the late 1960s, Hamel and Olson [8] synthesized the first dinitramide structure. These materials were covalently bonded alkyl N,N-dinitramides. The resulting dinitramides were unstable and decomposed at 75 °C or less, making them unsuitable as propellant ingredients. Recently new classes of inorganic oxidizers have been synthesized [9–11]. This class of oxidizer incorporates the newly discovered dinitramidate $[N(NO_2)_2{}^-]$ anion. The dinitramide acid and its salts are thermally more stable than the original alkyl N,N-dinitramides discovered in the late 1960s. One promising oxidizer from this class of compounds is ammonium

* Corresponding author. Tel.: +81 50 3362 5956; fax: +81 42 759 8284.
E-mail addresses: rachid.amrousse@jaxa.jp, rachid.amrousse@yahoo.fr (R. Amrousse).

0926-3373/$ – see front matter © 2012 Elsevier B.V. All rights reserved.
http://dx.doi.org/10.1016/j.apcatb.2012.08.009

dinitramide; abbreviated ADN, $N_4O_4H_4$ which has the structural formula $NH_4N(NO_2)_2$. ADN as ammonium nitrate (AN) undergoes residueless combustion. However, it burns more readily and predictably than AN. Therefore, it is much more attractive to use ADN as an ingredient in propellants than AN. Several solid propellant formulations of ADN in various binder systems have recently been accomplished [12,13]. Although, it is well known that dinitramides are energetic compounds, the thermal and catalytic decompositions of dinitramides have not been studied extensively at liquid state. ADN is a relatively new oxidizer which may be environmentally friendly because it does not have a halogen acid decomposition product. The decomposition reactions of ADN have been discussed by many researchers [14–16].

The principle objective of this work was to study and compare the behavior of binary HAN and ADN aqueous solutions displaying different mass concentrations, for thermal and catalytic decomposition using the catalytic materials developed for both monopropellants, i.e. Ir and copper oxide (CuO) supported on modified alumina by lanthanum oxide (La_2O_3). Moreover, the influence of the HAN and ADN concentrations on the decomposition processes was also discussed.

2. Experimental

2.1. Monopropellants

Binary $HAN_{95\%}$ was prepared by Hosoya Company (Tokyo, Japan) following controlled reaction between a concentrated aqueous solutions of hydroxylamine (50 wt.%) and nitric acid (65 wt.%).

$$NH_2OH(aq) + HNO_3(aq) \rightarrow NH_3OHNO_3(aq) \quad (1)$$

Binary $HAN_{80\%}$ and $HAN_{60\%}$ were prepared by dilution of $HAN_{95\%}$ stock solution.

ADN in crystalline state (purity 97%) was prepared in ISAS (Institute of Space and Astronautical Science, Kanagawa, Japan). This material used to prepare $ADN_{75\%}$, $ADN_{60\%}$ and $ADN_{50\%}$ by dissolution in pure water. Moreover, water in the system is reported to work simply as monopropellant stabilizer; however water will affect the oxidation state of the active metals.

2.2. Catalyst preparation

The alumina doped by La_2O_3 was synthesized using sol–gel procedure. At first, the preparation of colloidal solution was carried out at room temperature by mixing a known volume of nitric acid to control the pH solution, Disperal boehmite (Sasol, $S_{BET} = 260\ m^2\ g^{-1}$) and urea ($OC(NH_2)_2$). Urea, which is in the form of white pellets, is added to the beaker containing nitric acid. The urea is dispersed at high velocity: 6200 rpm for 5 min. The addition of boehmite (very fine white powder) is then performed in small quantity for 20 min under high mixing speed: 17,600; 21,700 and 23,000 rpm using an Ultra Turax T25 mixer. The lanthanum nitrate hexahydrate $La(NO_3)_3$ precursor (Wako, 99%) was dissolved in appropriate solution of pure ethanol. Lanthanum concentration was 10 wt.% of La_2O_3. Finally, thermal treatment of the prepared doped-colloidal suspension at 500 °C was carried out under air.

This step aims to develop a doped-porous layer thus promoting a better dispersion of the metal or oxide active phases. It was believed that the high surface area of doped-alumina support was necessary to maintain a superior catalytic performance in high temperature catalytic applications. Ir and CuO active phases were introduced onto the surface of the calcined support through the impregnation procedure with an excess of solvent (water), using aqueous solutions of hexachloroiridic acid H_2IrCl_6 (Wako) and copper (II) nitrate trihydrate $Cu(NO_3)_2$ (Wako, 99.9%). After drying at 60 °C, O_2-calcination and H_2-reduction at 500 °C led to the formation of Ir nano-size particles. Moreover, the $Cu(NO_3)_2$ was dried at room temperature for 24 h, then at 100 °C for 12 h, and finally treated at 500 °C in air for 8 h.

2.3. Catalyst characterization

The specific surface area was obtained through Brunauer, Emett and Teller (BET) measurements by using a Micromeritics Flowsorb II apparatus with the following conditions: 6 h pretreatment at 250 °C under nitrogen flow; N_2 in He with $P(N_2) = 0.3$ bar.

Moreover, both prepared catalysts were characterized by X-ray diffraction (XRD), mass 400–600 mg of finely ground powders was placed in a holder standard sample. This holder rotates about a vertical axis during measurement. In this case, the crystallites are oriented in a random manner and no direction of diffraction is preferred. The XRD patterns were recorded in domain 2θ between 5° and 90° with a step of 0.06° and an acquisition time of 2 s.

Transmission electron microscope (TEM) Philips CM120 has been used with a resolution of 3.5 Å. The catalysts were milled, put in ethanol solution, dispersed with ultra sound and deposited on a copper grid; then carbon was deposited. Several photos corresponding to different parts of the sample were taken and the distribution in size was obtained by manually counting on 5–10 pictures in order to obtain a good statistical distribution. Finally, Ir accessibility has been evaluated from hydrogen chemisorption at room temperature using pressure measurements. The sample (500 mg) are reduced at 400 °C during 1 h and cooled at room temperature. The adsorption isotherms lead to the determination of reversible and irreversible adsorbed hydrogen. The dispersion is calculated using the stoichiometric ratio H/Ir = 1.

2.4. Monopropellant decomposition

The monopropellant decomposition processes were followed using two reactor facilities: a thermal analysis apparatus (TA Instrument, Q600) and a constant volume batch reactor. For the thermal analysis (thermogravimetric analysis and differential thermal analysis, DTA–TG), 8 mg of catalyst are put into an aluminum sample holder, followed by the addition of 5 μL of aqueous monopropellant solution and covered with a cap. The mass and temperature are recorded versus time, with a temperature ramp of 10 °C min^{-1} under an argon flow (100 mL min^{-1}). Analyses by DTA–TG enable us to obtain the following information: (i) onset temperature of decomposition given by the inflexion point of the temperature curve; (ii) concentration of the HAN solution at decomposition and (iii) efficiency of the catalyst (exothermic peak).

In the constant volume batch reactor already described [17,18], the monopropellant (50 μL) is added to the catalyst (80 mg) at room temperature under 1 bar of argon flow, using a microsyringe through a septum, and then heated with a slope of 10 °C min^{-1}. The pressure and temperature for gaseous phases are recorded versus time. This reactor has been built to acquire data on the catalytic decomposition reaction of different monopropellants and catalysts at low temperature. The catalyst can be preheated in the 20–250 °C range, and two operation modes are achieved: constant temperature mode and temperature increase mode. Moreover, the catalyst can be heated with a fixed heating rate or preheated at a defined temperature. It is placed inside a specific sample holder, which prevents the loss of sample after possible ejections during the exothermic decomposition. The monopropellant is added through a microsyringe (100 μL). Between successive monopropellant injections, the decomposition products can be quickly evacuated through the vacuum line up to 3×10^{-2} mbar. This reactor can be used to simulate cold starts or injection by pulses, but not stationary monopropellant flow (steady-state studies).

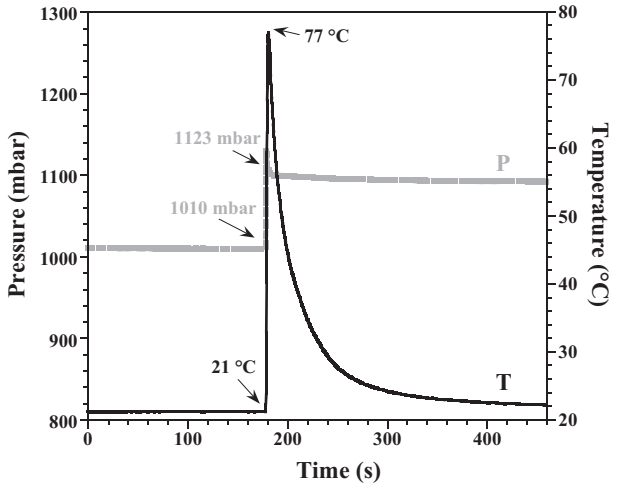

Fig. 1. Catalytic decomposition of binary $HAN_{95\%}$ aqueous solution in the batch reactor, catalyst: (10%)Ir/Al_2O_3–La_2O_3.

Fig. 1 shows the catalytic decomposition of binary $HAN_{95\%}$ solution. The ignition temperature of the propellant decomposition is easily determined (21 °C), the reaction rate can be calculated between the maximum and minimum points (285 mbar s^{-1}) and demonstrates the catalyst efficiency. The injection of 50 μL corresponds to a mass of 0.81 mg ($\rho = 1.618\ g\ cm^{-3}$) of propellant containing 0.80 mmol of HAN (95 wt.%; $M_{HAN} = 96.04\ g\ mol^{-1}$). The decomposition reaction involves a sharp pressure increase associated with a temperature rise, due to the formation of gaseous products as shown by possible Eqs. (2)–(5) (Fig. 2):

$$NH_3OHNO_3(aq) \rightarrow 2H_2O(l) + N_2(g) + O_2(g) \quad (2)$$

$$NH_3OHNO_3(aq) \rightarrow 2H_2O(l) + 0.5N_2(g) + NO_2(g\ or\ l) \quad (3)$$

$$NH_3OHNO_3(aq) \rightarrow 2H_2O(l) + 2NO(g) \quad (4)$$

$$NH_3OHNO_3(aq) \rightarrow 2H_2O(l) + N_2O(g) + 0.5O_2(g) \quad (5)$$

Nitric acid was proposed as intermediate reaction species [19], but we did not observe its quantitative formation in the final products, the pH of residual water being 2.3, due probably to the dissolution of nitrogen dioxide. The thermodynamics products (Eq. (2)) correspond to a molar ratio $n_{gas}/n_{HAN} = 2$. Eqs. (3)–(5) display the formation of kinetic products. For Eq. (3) [20], the ratio n_{gas}/n_{HAN} is only 0.5 taking into account the strong water solubility of NO_2. For Eq. (4) [21], the molar ratio is 1.50, thus showing the strong difference between these processes and the need to know quantitatively all products formed during the decomposition reactions.

The gaseous mole number released during the decomposition is calculated by using perfect gas law (Eq. (5)) and taking into account the volume of the reactor (160 cm^3), the pressure increase and the temperature of the gas phase. As an example, Fig. 1 corresponds to a gas mole rise of 0.74 mmol, thus giving n_{gas}/n_{HAN} ratio of 0.93. This ratio discloses the formation of kinetic products N_2O, NO and NO_2, which was proved using a reactor facility with online analysis by mass spectrometer [22].

In conclusion, the catalytic activities can be related to the pressure increase, the decomposition onset temperature and the reaction rate.

3. Results and discussion

3.1. Catalysts characterization

Ir and CuO do not change the texture of doped-alumina, the BET surface area (230 and 228 $m^2\ g^{-1}$ respectively; Table 1) remaining close to the value obtained for the support before impregnation (232 $m^2\ g^{-1}$). Therefore, the specific surface areas of Ir-based and CuO-based catalysts have been almost similar to that of the corresponding support, indicating that the texture of the alumina is not modified by the impregnation and heat treatment and that the active phase particles were involved in the contribution of the surface area of catalysts. In addition, the porous volume was lower than those of the support after the incorporation of the active phase. This can be explained by blocking (or occupation) of small pores by the Ir and CuO crystallites (partial filling of the pores) and/or by rapid saturation of the support with the metal salt precursors.

The determination of Ir and CuO contents (9.3 and 8.5% respectively) indicates a loss of both active phases by comparison with calculated values (10%), due to the thermal treatment step.

The structural data from X-ray diffraction confirm the presence of γ-Al_2O_3 (JCPDS: 050-0741), Ir metal phase (JCPDS: 087-0715) and CuO (JCPDS: 048-1548). The characteristic peaks of La_2O_3 are absents in these patterns due to its low mass percentage (10 wt.%) on the support.

Moreover, the evident broadening of the corresponding diffraction peaks of the Ir and CuO on the doped-alumina indicating that the Ir and CuO crystal particles have high dispersion on the doped-alumina support with much smaller sizes and crystallite form. Nano-sized crystallites will produce more crystal lattice defects, which usually are the highly active sites. The determination of Ir and CuO crystallite size (Table 1) is based on the two basic diffraction

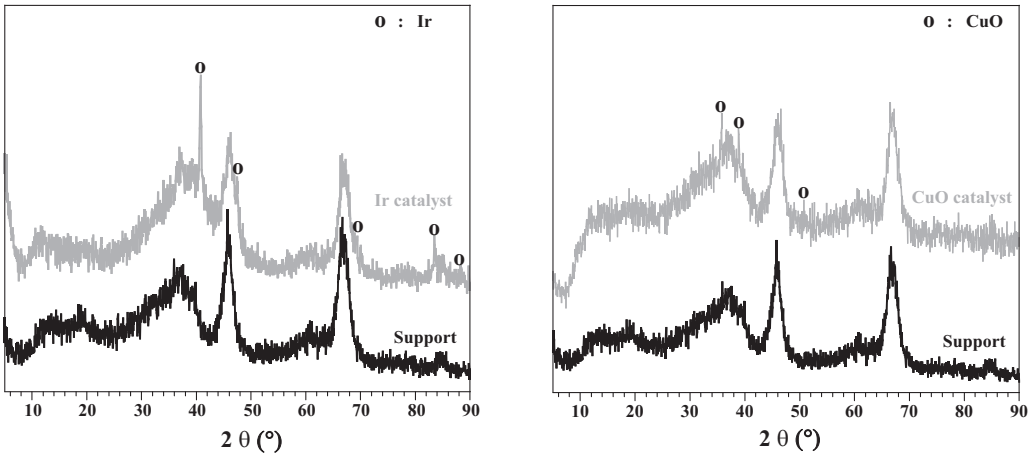

Fig. 2. XRD patterns of Ir-based and CuO-based catalysts.

Table 1
Structural data, specific surface area and catalyst particle sizes (*S*).

Structure	BET ($m^2\ g^{-1}$)	Calculated %	Experimental %	S_{XRD} (nm)	$S_{chemisorption}$ (nm)
Ir/γ-Al_2O_3	230	9.3	10	6	8
CuO/γ-Al_2O_3	228	8.5	10	14	–

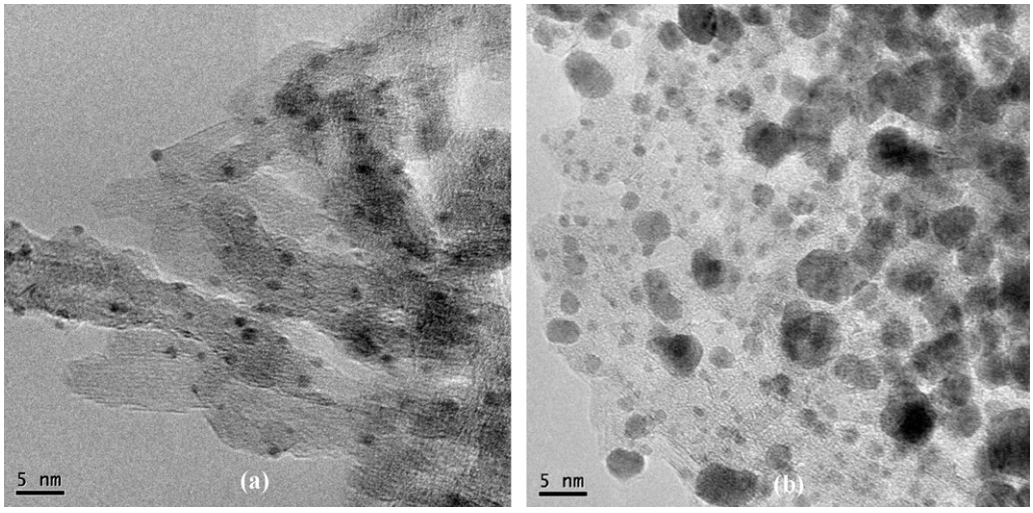

Fig. 3. TEM images of: (a) Ir-based catalyst and (b) CuO-based catalyst.

peaks (more intense), which show no disturbance from the support phase. For Ir-based catalyst, the crystallite size value is in agreement with the hydrogen chemisorption analysis (cubic model).

The present particles on the TEM images were measured to determine the particle distribution size. We calculate the particle average sizes on the surface by the relationship $d = \sum n_i d_i^3 / \sum n_i d_i^2$. Fig. 3 shows the TEM images of Ir and CuO-based catalysts, these images show that Ir particles are distributed homogeneously on the modified-alumina support. On the other hand, CuO particles are distributed heterogeneously, due to low interaction between oxide active phase and doped-support. In addition, several parameters can influence these sizes, such as the preparation method of the support, the heat treatment temperatures, and the gas flow rates. The histogram of particle size distributions of Ir and CuO-based catalysts is reproduced (not presented). Indeed, a number of fairly large CuO particles were measured. The contribution of these particles leads to average sizes of about 2 and 8 nm for Ir and CuO particles, respectively. Since active components with smaller particle sizes give higher catalytic activity (Doyle et al. [23]), therefore the nano-particles of Ir and CuO will increase the surface area and offer a high density of surface active sites to promote catalytic decomposition of HAN and ADN liquid monopropellant, respectively.

3.2. Monopropellant characterization

Raman spectrums of $HAN_{95\%}$ and $ADN_{75\%}$ are shown in Fig. 4.

The Raman spectrum of HAN–water (Fig. 4a) has been recorded at ambient temperature and shows the presence of the characteristic peak of NO_3^- and NH_3OH^+ entities. This spectrum is mainly characterized by the presence of two lines corresponding to the stretching vibrations of N—OH entities and NO_3^- located respectively at 1010 and 1050 cm^{-1} [24,25]. In addition, the broad bands located between 3100 and 3500 cm^{-1} correspond to the vibration modes of O–H of H_2O and HAN in agreement with literature data [26–31]. In addition, the region 2700–3000 cm^{-1} contains the signatures of N—H stretching modes of NH_3OH^+ cation of HAN. The intense low peak located at 1599 cm^{-1} can be attributed to the

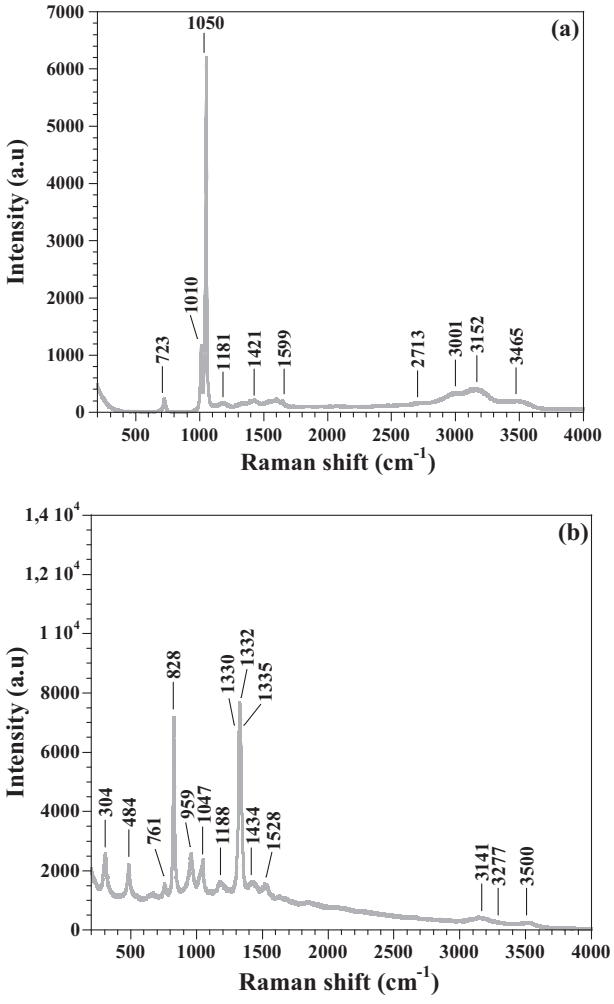

Fig. 4. Raman spectrums of: (a) $HAN_{95\%}$ and (b) $ADN_{75\%}$ at room temperature.

deformation mode of $\delta(NH_3)$ of NH_3OH^+ cation [24,25]. The nitrate anion NO_3^- is characterized by the presence of three peaks: the first, wide and low at 1421 cm^{-1} corresponds to the antisymmetric stretching, the second, very strong, is located at 1050 cm^{-1} and corresponds to the symmetric stretching, while the third, located at 723 cm^{-1}, corresponds to the strain mode of NO_3^- anion. The peak located at 1010 cm^{-1} corresponds to the stretching vibration of N—OH band. The peak located at 1181 cm^{-1} is due to the presence of OH group [32–34]. Moreover, the Raman spectrum of binary ADN–water mixture (Fig. 4b) has been recorded. It reveals the presence of the characteristic peaks which can be assigned to NO_2 and N_3 (N—N—N) vibrations. Indeed, the weak peaks located at 1528; 1434 and 1188 cm^{-1} and the strong peak located at 1332 cm^{-1} originate from NO_2 stretching vibrations. Moreover, the medium peak located at 1047 cm^{-1} is attributed to N—N stretching mode. The medium peak located at 959 cm^{-1} results from a superimposition of N—N stretching and N—N—N bending mode. The broad band in the 3200–3600 cm^{-1} region is assigned to the OH group of H_2O, whereas, the shoulder at 3141 cm^{-1} is assigned to NH_4^+ stretching mode [35].

3.3. Thermal decomposition

The thermal decomposition followed by thermal analysis of 5 μL of $HAN_{95\%}$ and $ADN_{75\%}$ aqueous solutions is given in Fig. 5.

The HAN thermal behavior is different to ADN thermal behavior. Indeed, HAN thermal behavior has an endothermic peak corresponding to the evaporation of 5% of H_2O, resulting in concentration of solution and following by to exothermic peaks correspond to HAN decomposition in two steps. However, binary ADN decomposes in one step after an endothermic peak corresponding to the evaporation of 25% of H_2O. The exothermic decompositions in both cases correspond to neat HAN or ADN liquid leading to the complete transformation of the propellant into gaseous phase products. The decomposition temperatures are: 155 °C for $HAN_{95\%}$ and 116 °C for $ADN_{75\%}$ respectively. The decomposition starts only when the solvent (water) has been quantitatively removed leading to almost pure liquid HAN (melting point 48 °C) or ADN (melting point 92 °C). From these results, we can conclude that water exhibits, as expected, a stabilizing effect on HAN or ADN, which is the consequence of dispersed ions in solutions. The ionic reagents must therefore be in contact with each other for decomposition to engender. Mostly, literature data gives approximately similar data for HAN [36], which were observed in our study.

The exothermic peak is most rapid and higher for ADN (224 °C as maximum temperature), indicating a greater energy release or reaction rate by comparison with HAN (218 and 206 °C as maximum temperatures). Both solutions were tested in the batch reactor facility (Fig. 6); as the thermal analysis results, decomposition occurs at a lower temperature for $ADN_{75\%}$ (116 °C) by comparison with $HAN_{95\%}$ (152 °C). The pressure increase for $ADN_{75\%}$ decomposition (ΔP = 147 mbar) is lower than $HAN_{95\%}$ (ΔP = 202 mbar) and the reaction displays a higher rate (slope value is 103 mbar s^{-1} for $ADN_{75\%}$ versus 106 mbar s^{-1} for $HAN_{95\%}$). The decomposition reaction is represented by Eqs. (2)–(5) for HAN and by Eq. (6) for ADN (thermodynamic products):

$$NH_4N(NO_2)_2(aq) \rightarrow 2N_2(g) + 2H_2O(l) + O_2(g) \quad (6)$$

Therefore, the decomposition products are different which implies different gaseous mole numbers and different pressure increase values, which cannot be compared. All data of the different monopropellant solutions are brought together in Table 2.

3.4. Catalytic decomposition

The catalytic decomposition of the two propellants $HAN_{95\%}$ and $ADN_{75\%}$ with (10%)Ir and (10%CuO)-based catalysts respectively were first followed by thermal analysis, of 5 μL of $HAN_{95\%}$ with 8 mg of Ir-based catalyst and $ADN_{75\%}$ with 8 mg of CuO-based catalyst (Fig. 7). Weight losses reached at the end of the reaction processes are similar from expected data, due to the high exothermicity of the decomposition, which ejects a small amount of catalysts outside the sample holder. For both solutions, very high exothermic peaks are observed in one step (fast decompositions) followed by small endothermic peaks indicating a low energy release due to the presence of H_2O as decomposition product. Nevertheless, the catalyst efficiencies are demonstrated by the important reaction temperature decrease: 47 °C instead of 155 °C for thermal process of $HAN_{95\%}$ and 51 °C instead of 116 °C for thermal decomposition of $ADN_{75\%}$.

Whatever the mixture, the pressure increase measured in the batch reactor (Fig. 8) remains always very low. In presence of HAN and ADN, the pressure variation is attributed to H_2O and N_2O [37].

This proposal hypothesis will be checked by on-line gas analysis of different products after catalytic decomposition.

The complete results are given in Table 3. The catalytic effect is clearly evidenced by decomposition temperature decrease, by comparison with thermal reaction (compare with Table 2). As the thermal decomposition results, the temperature of HAN and ADN catalytic reaction decreases and the rate rises when the concentration increases.

Catalytic decomposition of the binary $HAN_{95\%}$ and $ADN_{75\%}$ solutions occur at room temperature. The pressure increase obtained with $HAN_{95\%}$ solution is larger than that of $ADN_{75\%}$ solution despite the lower decomposition temperature, indicating a much efficient catalytic reaction and a higher decomposition rate (Table 3). These

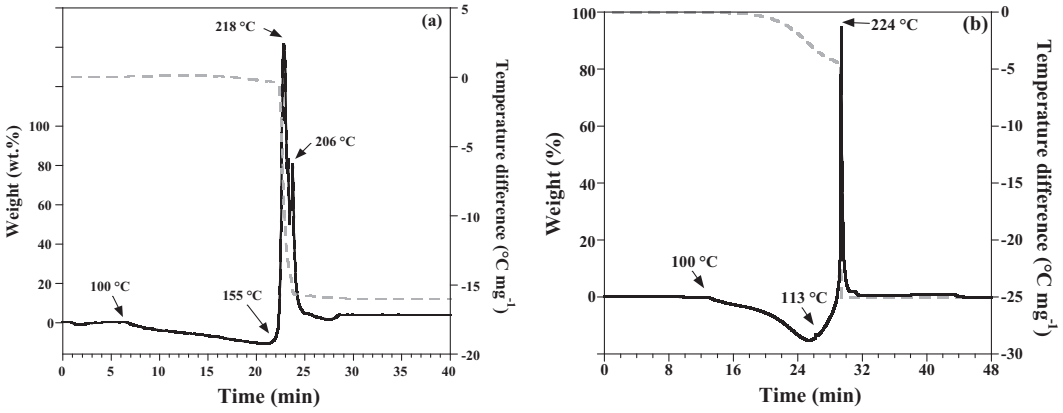

Fig. 5. Thermal decomposition of binary: (a) $HAN_{95\%}$ and (b) $ADN_{75\%}$ solutions by DTA–TG.

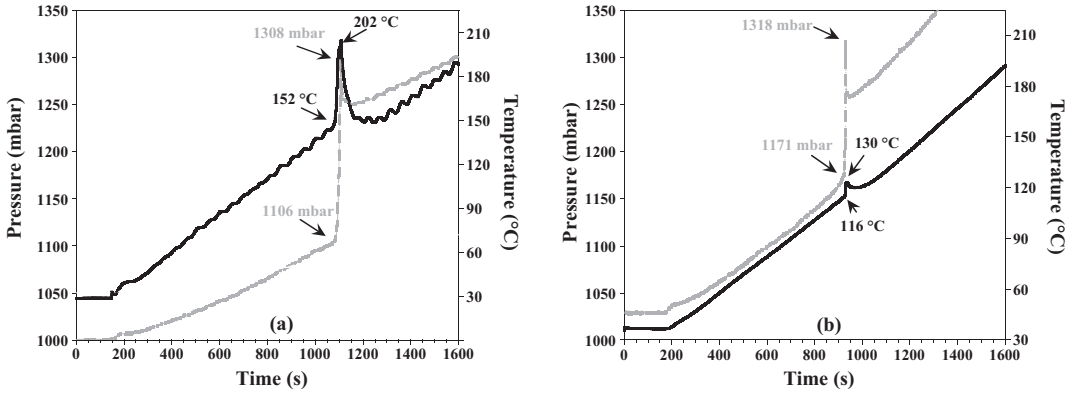

Fig. 6. Thermal decomposition of binary: (a) $HAN_{95\%}$ and (b) $ADN_{75\%}$ solutions in the batch reactor facility.

Table 2
Experimental data after thermal decomposition processes of binary HAN and ADN mixtures.

	HAN–water			ADN–water		
Weight percentage (wt.%)	95	80	60	75	60	50
Density (g cm^{-3})	1.618	1.514	1.393	1.526	1.422	1.312
T_{dec} DTA–TG (°C)	155	167	175	116	128	152
T_{dec} batch reactor (°C)	152	164	173	113	124	150
T_{gas} (°C)	202	193	178	130	105	92
ΔP (mbar)	202	192	166	147	135	128
Rate (mbar s^{-1})	106	101	87	103	94	89
n_{gas} (mmol)	0.91	0.85	0.72	0.73	0.65	0.58
$n_{gas}/n_{propellant}$	1.14	1.35	1.64	1.59	1.91	2.23

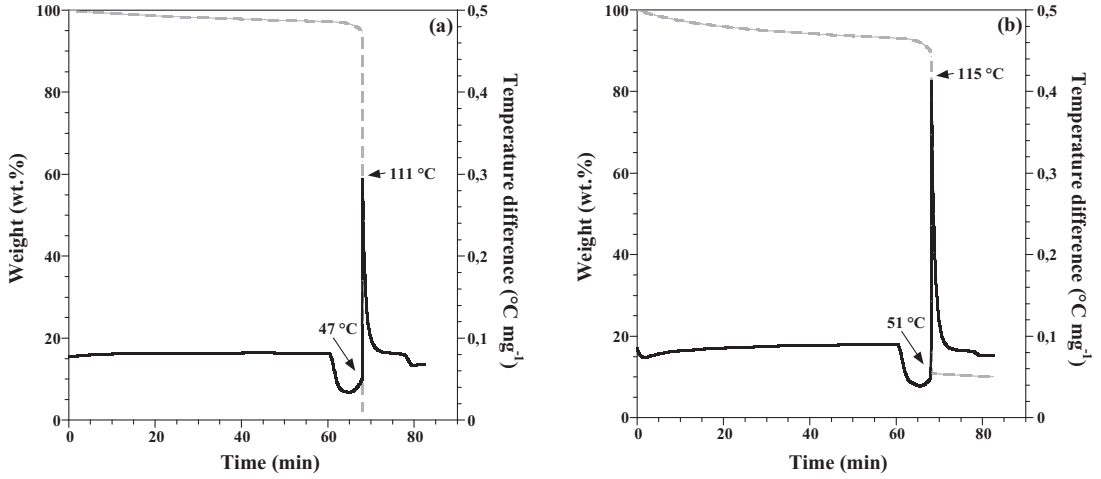

Fig. 7. Catalytic decomposition of binary: (a) $HAN_{95\%}$ and (b) $ADN_{75\%}$ solutions by DTA–TG.

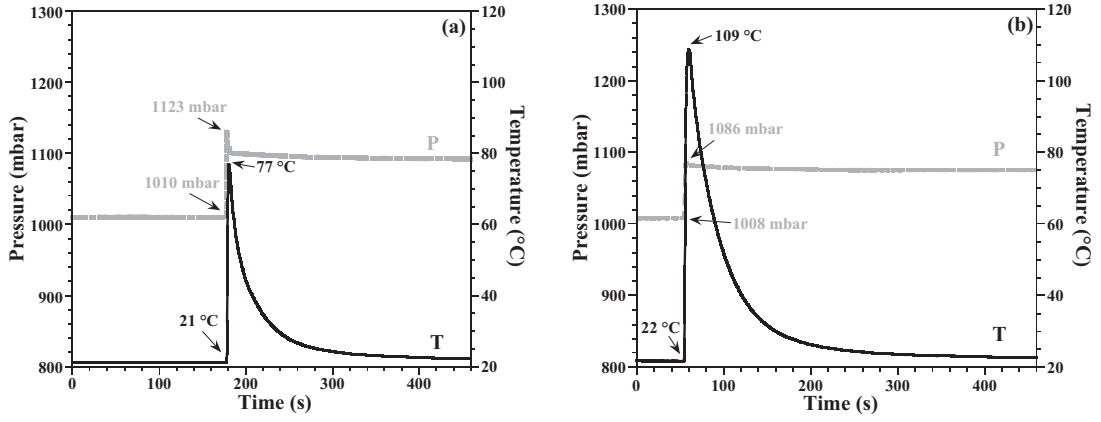

Fig. 8. Catalytic decomposition of binary: (a) $HAN_{95\%}$ (Ir-based catalyst) and (b) $ADN_{75\%}$ (Cu-based catalyst) solutions in the batch reactor facility.

Table 3
Experimental data after catalytic decomposition processes of binary HAN and ADN mixtures.

	HAN–water			ADN–water		
Weight percentage (wt.%)	95	80	60	75	60	50
T_{dec} DTA–TG (°C)	47	51	72	51	71	78
T_{dec} batch reactor (°C)	21	42	69	22	45	74
T_{gas} (°C)	77	75	72	109	100	93
ΔP (mbar)	113	104	92	78	75	69
Rate (mbar s^{-1})	285	260	230	78	74	71
n_{gas} (mmol)	7.4	6.4	5.2	5.1	4.5	3.8
$n_{gas}/n_{propellant}$	9.25	10.2	11.8	11.1	13.2	14.6

differences can be explained by the nature of obtained gaseous products and catalyst activities. Effectively, Ir and CuO supported on La_2O_3-doped alumina must be improved to be used with $ADN_{75\%}$ and $HAN_{95\%}$ respectively.

The mole number of gas ejected during the thermal and catalytic decompositions are given in Fig. 9. Whatever the solution, the gas mole numbers for catalytic decomposition process remains most important than thermal reaction. The best results are obtained for the most concentrated solutions. Although these catalysts are more efficient for decomposing $HAN_{95\%}$ and $ADN_{75\%}$ solutions. They are enable higher gas mole numbers than for thermal processes, which are encouraging.

Very good activities are demonstrated by low decomposition temperatures, fast reaction rates and large amounts of gaseous phase products released during the reaction. Low decomposition temperatures avoid preheating of reaction control system, thus reducing costs and energy supply. From these results, the best catalyst/monopropellant combinations are (10%)Ir/Al_2O_3–La_2O_3 associated with $HAN_{95\%}$ and (10%)CuO/Al_2O_3–La_2O_3 with $ADN_{75\%}$.

All these experiments display the very good activity and stability of both catalysts. Indeed they allowed the efficient decomposition of the HAN/water solution at low temperature even in the presence of a large amount of solution. Moreover, these materials remain active, showing a high reaction rate and an important pressure increase, after monopropellant injections which remain a challenge for the development of new satellites thrusters. The feature work will focus on the mechanism studies of HAN and ADN catalytic decompositions.

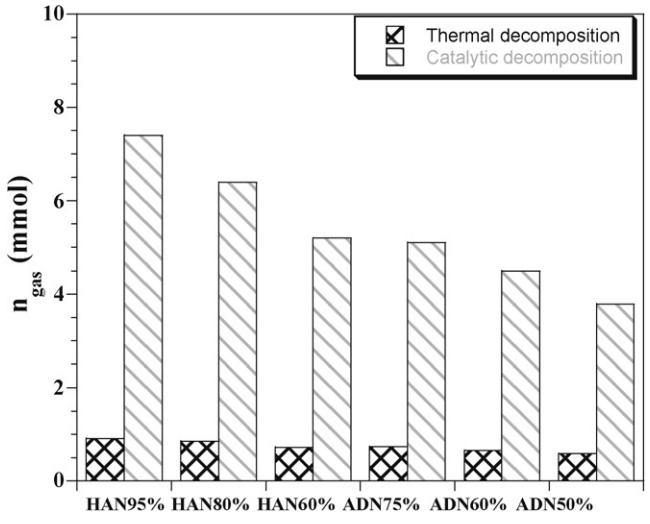

Fig. 9. Molar quantities of gas ejected during thermal and catalytic decomposition of monopropellants.

4. Conclusion

For both monopropellants, the thermal decomposition starts only when water has been completely evaporated, the onset temperature is 152 °C for the $HAN_{95\%}$ solution and 113 °C for the $ADN_{75\%}$ solution using the batch reactor facility. HAN thermal decomposition shows a higher exothermic peak than ADN indicating that more energy is released. The presence of appropriate catalytic active phases lead to a drop of the onset temperature, revealing that decomposition can be triggered at lower temperature, even in the presence of water. In addition, the reaction rate is larger by comparison with the thermal decomposition. HAN and ADN catalytic decomposition manifest a single step at low temperatures. Finally, the concentration effect of HAN and ADN solutions was demonstrated. Indeed, the best results (low decomposition temperature, sharp rise of pressure and reaction rate) were obtained for the more concentrated binary aqueous solutions.

Acknowledgments

Dr. Rachid Amrousse would like to thank Japan Aerospace Exploration Agency for financial support, Hosoya Company (Tokyo, Japan) for preparation of HAN solution and Mr. Kohji Fujisato (Tokyo University, Japan) for ADN preparation.

References

[1] L. Courthéoux, D. Amariei, S. Rossignol, C. Kappenstein, European Journal of Inorganic Chemistry 12 (2005) 2293–2295.
[2] O.M. Morgan, D.S. Meinhardt, Proceeding of 35th AIAA/ASME/SAE/ASEE Joint Propulsion Conference and Exhibit, AIAA-2595, Los Angeles, CA, 1999.
[3] L. Courthéoux, F. Popa, E. Gautron, S. Rossignol, C. Kappenstein, Journal of Non-Crystalline Solids 350 (2004) 113–119.
[4] L. Courthéoux, D. Amariei, S. Rossignol, C. Kappenstein, N. Pillet, M. Ford, Proceedings of Space Propulsion 2004, The 2nd International Conference on Green Propellants for Space Propulsion, Sardinia, Italy, 2004.
[5] K. Hisatsune, J. Izumi, H. Tsutaya, K. Furukawa, Proceedings of Space Propulsion 2004, The 2nd International Conference on Green Propellants for Space Propulsion, Sardinia, Italy, 2004.
[6] A.J. Fortini, J.R. Babcock, Proceedings of 37th AIAA/ASME/SAE/ASEE Joint Propulsion Conference and Exhibit, AIAA-3393, Salt Lake City, UT, 2001.
[7] D. Zube, S. Christofferson, E. Wücherer, B. Reed, Proceedings of 39th AIAA/ASME/SAE/ASEE Joint Propulsion Conference and Exhibit, AIAA-4643, Huntsville, Alabama, 2003.
[8] E.E. Hamel, R.E. Olson, US Patent 3,428,667 (1969).
[9] J.C. Bottaro, R.J. Schmidt, P.E. Penwell, D.S. Ross, US Patent 5,198,204 (1993).
[10] J.C. Bottaro, R.J. Schmidt, P.E. Penwell, D.S. Ross, US Patent 5,254,324 (1993).
[11] R.J. Schmidt, J.C. Bottaro, P.E. Penwell, D.C. Bomberger, US Patent (2001).
[12] C. Hinshaw, R.B. Wardle, T.K. Higshmith, US Patent 5,498,303 (1998).
[13] Z. Pak, Proceedings of 29th AIAA/ASME/SAE/ASEE Joint Propulsion Conference and Exhibit, AIAA-1755, Monterey, CA, 1993.
[14] T.P. Russell, A.G. Stern, W.M. Koppes, C.D. Bedford, CPIA, Publ. II, 1992, p. 339.
[15] J.C. Oxley, J.L. Smith, W. Zheng, E. Rogers, M.D. Coburn, Journal of Physical Chemistry A 101 (1997) 5646–5652.
[16] S. Vyazovkin, C.A. Wright, Journal of Physical Chemistry A 101 (1997) 5653–5658.
[17] R. Eloirdi, S. Rossignol, M. Chauveau, C. Kappenstein, D. Duprez, N. Pillet, Proceedings of the 36th AIAA/ASME/SAE/ASEE Joint Propulsion Conference and Exhibit, AIAA-3553, Huntsville, AL, 2000.

[18] R. Eloirdi, S. Rossignol, C. Kappenstein, D. Duprez, N. Pillet, Journal of Propulsion and Power 19 (2003) 213–219.
[19] J. Cronin, T. Brill, Journal of Physical Chemistry A 90 (1986) 178–181.
[20] H. Lee, T.A. Litzinger, Combustion and Flame 135 (2003) 151–169.
[21] R.A. Sasse, Report No. BRL-MR-3651, Order No. AD-A193893, 1988.
[22] Y. Batonneau, L. Courthéoux, P. Esteves, L. Pirault-Roy, S. Rossignol, C. Kappenstein, N. Pillet, Proceedings of the 40th AIAA/ASME/SAE/ASEE Joint Propulsion Conference and Exhibit, AIAA-3835, Fort-Lauderdale, FL, 2004.
[23] D.M. Doyle, G. Palumbo, K.T. Aust, A.M. EL-Sherik, U. Erb, Acta Metallurgica et Materialia 43 (1995) 3027–3033.
[24] D.L. Frasco, E.L. Wagner, Journal of Chemical Physics 30 (1959) 1124–1130.
[25] C. Rocchiccioli, Comptes Rendus Mathematique 253 (1961) 838–842.
[26] G.E. McGraw, D.L. Bernitt, I.C. Hatsune, Journal of Chemical Physics 42 (1965) 237–244.
[27] G.E. Walrafen, Journal of Chemical Physics 55 (1971) 768–792.
[28] B.R.S. Sengar, G. Narain, Bulletin of the Chemical Society of Japan 48 (1925) 1087–1088.
[29] N.B. Colthup, L.H. Daly, S.E. Wiber-ley, Introduction to Infrared and Raman Spectroscopy, Academic Press, New York, 1975.
[30] Y. Yeh, J.H. Biigram, W. Kanzig, Journal of Chemical Physics 77 (1982) 2317–2321.
[31] P.A. Giguere, J.G. Guillot, Journal of Physical Chemistry 86 (1982) 3231–3233.
[32] R.E. Hester, R.A. Plane, Journal of Chemical Physics 40 (1964) 411–414.
[33] D.E. Irish, G.E. Walrafen, Journal of Chemical Physics 46 (1967) 378–384.
[34] D.E. Irish, A.R. Davis, Canadian Journal of Chemistry 46 (1968) 943–951.
[35] K.O. Christe, W.W. Wilson, M.A. Petrie, H.H. Michels, J.C. Bottaro, R.D. Gilardi, Inorganic Chemistry 35 (1996) 5068–5071.
[36] L. Courthéoux, D. Amariei, S. Rossignol, C. Kappenstein, Applied Catalysis B 62 (2006) 217–225.
[37] L. Courthéoux, E. Gautron, S. Rossignol, C. Kappenstein, Journal of Catalysis 232 (2005) 10–18.